

The first broad-band X-ray images and spectra of the 30 Doradus region in the LMC^{*}

K. Dennerl¹, F. Haberl¹, B. Aschenbach¹, U. G. Briel¹, M. Balasini⁴, H. Bräuninger¹, W. Burkert¹, R. Hartmann¹, G. Hartner¹, G. Hasinger³, J. Kemmer⁶, E. Kendziorra², M. Kirsch², N. Krause¹, M. Kuster², D. Lumb⁵, P. Massa⁴, N. Meidinger¹, E. Pfeffermann¹, W. Pietsch¹, C. Reppin¹, H. Soltau⁶, R. Staubert², L. Strüder¹, J. Trümper¹, M. Turner⁷, G. Villa⁴, and V. E. Zavlin¹

¹ Max-Planck-Institut für extraterrestrische Physik, 85748 Garching, Germany

² Institut für Astronomie und Astrophysik der Univ. Tübingen, Waldhäuserstr. 64, 72076 Tübingen, Germany

³ Astrophysikalisches Institut Potsdam, An der Sternwarte 16, 14482 Potsdam, Germany

⁴ Istituto di Fisica Cosmica “G. Occhialini”, Via Bassini 15, 20133 Milano, Italy

⁵ XMM Science Operations Centre, Space Science Division ESTEC, Postbus 299, 2200 AG Noordwijk, Netherland

⁶ KETEK GmbH, Am Isarbach 30, 85764 Oberschleißheim, Germany

⁷ Physics and Astronomy Department, University of Leicester, Leicester LE1 7RH, United Kingdom

Received <date> / Accepted <date>

Abstract. We present the XMM–Newton first light image, taken in January 2000 with the EPIC pn camera during the instrument’s commissioning phase, when XMM–Newton was pointing towards the Large Magellanic Cloud (LMC). The field is rich in different kinds of X–ray sources: point sources, supernova remnants (SNRs) and diffuse X–ray emission from LMC interstellar gas. The observations are of unprecedented sensitivity, reaching a few 10^{32} erg/s for point sources in the LMC. We describe how these data sets were analysed and discuss some of the spectroscopic results. For the SNR N157B the power law spectrum is clearly steeper than previously determined from ROSAT and ASCA data. The existence of a significant thermal component is evident and suggests that N157B is not a Crab-like but a composite SNR. Most puzzling is the spectrum of the LMC hot interstellar medium, which indicates a significant overabundance of Ne and Mg of a few times solar.

Key words. Methods: data analysis – Techniques: image processing – ISM: abundances – ISM: supernova remnants – Galaxies: LMC – X–rays: ISM

1. Introduction

On December 10 1999 the XMM–Newton spacecraft was placed in a 48 hour Earth orbit by the first commercial ARIANE V launcher. XMM–Newton, or X–ray Multi–Mirror Mission (Jansen et al. 2001), is the second cornerstone of the Horizon 2000 science program of the European Space Agency ESA.

The EPIC pn camera (Strüder et al. 2001) was successfully commissioned during the period of mid January through mid March (Briel et al. 2000). On January 19 2000, shortly after the switch–on of the EPIC pn camera, XMM–Newton received first light on the EPIC pn CCD chip. We selected as first light target a region in the LMC about 10 arcmin southwest of the 30 Doradus A complex.

Send offprint requests to: K. Dennerl, e-mail: kod@mpe.mpg.de

^{*} Based on observations with XMM–Newton, an ESA Science Mission with instruments and contributions directly funded by ESA Member States and the USA (NASA)

The field has been known to be very rich in X–ray sources from Einstein (Long et al. 1981) and ROSAT observations (Trümper et al. 1991). There are at least three SNRs (one of those known to contain a pulsar), one OB association and two R associations as well as the SN 1987A. This XMM–Newton first light has already stimulated detailed studies of some of the objects. Here we report some results of the observation with four observation sequences of the same field added totaling an exposure time of 106 ks. The observations are of unprecedented sensitivity, reaching a few 10^{32} erg/s for point sources. We present and discuss the spectroscopic results over the broadest X–ray band-pass of 0.3–12 keV ever covered by a single imaging X-ray instrument for the entire field of 27×27 arcmin². In section 2 we describe details of the data analysis techniques which may be useful for other observations as well. In section 3 we discuss some of the scientific results.

Table 1. Journal of Observations

Date	Time	RA(2000)	DEC(2000)
2000 Jan 19	16:19 – 17:23	05 36 57.0	-69 13 47
2000 Jan 19/20	17:30 – 04:28	05 36 57.0	-69 13 47
2000 Jan 21	15:38 – 19:38	05 37 04.0	-69 13 00
2000 Jan 21/22	20:32 – 07:01	05 37 04.0	-69 13 00
2000 Jan 22	09:08 – 12:02	05 36 04.0	-69 13 00

2. Observations and Data Reduction

The region in the LMC was observed with the pn CCD camera operating in full frame mode (frame time: 73 ms), with the medium and thin filter inserted during the first three and last two observations, respectively (Strüder et al. 2001 and Turner et al. 2001). In Tab. 1 we show the journal of the observations. For a fixed pointing direction some photons fall onto the gaps between adjacent CCD chips. Fortunately, the pointing direction and the roll angle were changed for the later three observations with about the same exposure time as for the previous two observations, such that the surface brightnesses are within a factor of 2, with any noise contribution negligible. The data analysis was performed with software which was developed for the analysis of ground calibration measurements of the EPIC pn camera (Dennerl et al. 1999). Most of this software has been implemented into the XMM Standard Analysis Software (SAS, Watson et al. 2001).

During the observations the background induced by low energy protons changed and reached sometimes count rates of several hundred counts per second in the full energy band. To enhance the signal to noise ratio, we screened the observations for times with high background and excluded those times from further processing. The net observing time after screening is 54.8 ks. In addition the trails of minimum ionizing particles and reemission trails were removed frame by frame. The remaining events were corrected for charge transfer loss and gain variations, and events created by a single photon, but split across several pixels, were recombined, to yield a photon event file in detector coordinates with corrected energies (see Dennerl et al. 1999 for a detailed description).

Test images produced from this data set in various energy bands indicated that the energy range $E = 0.3 - 5.0$ keV was optimal to provide clean images with high signal to noise ratio. The energy range was then split into three narrower bands of similar signal to noise ratio, to create red, green and blue components of the final rgb image. The variation in spectral hardness of the LMC sources and the spectral resolution of the EPIC pn camera resulted in colourful images which, however, do not represent the dynamic range in intensity very well. To preserve the flux information as well, the colour saturation was reduced by choosing overlapping energy ranges (0.3–1.0 keV for red, 0.8–2.0 keV for green, and 1.5–5.0 keV for blue), and by further distributing some of the flux from these bands into other bands.

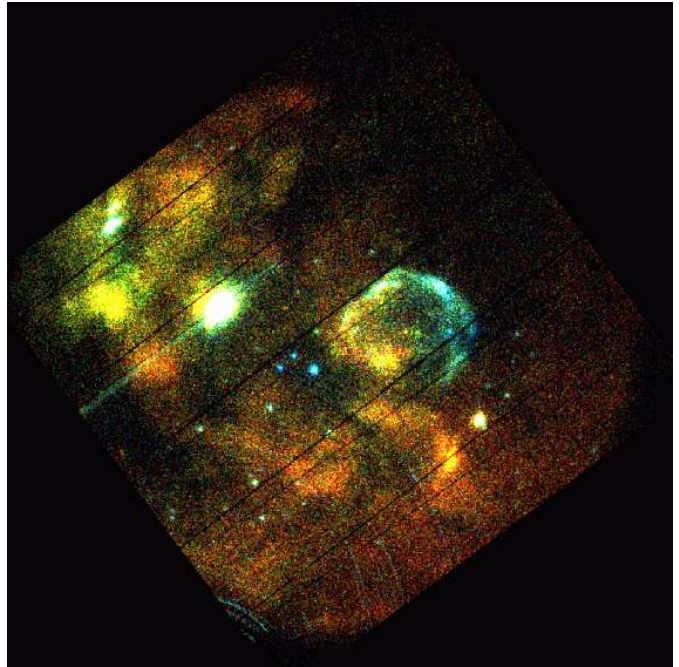


Fig. 1. Superposition of the photons detected with the EPIC pn camera in all five LMC observations, displayed in equatorial coordinates. The photon energy is coded in colour, ranging from 0.3 keV (red) to 5.0 keV (blue). As this image has not been corrected for exposure variations, the CCD boundaries are visible. The SNR N157B, the brightest source in the image, is saturated; an out-of-time event trail extends along the CCD column where the central neutron star is located. In the lower part of the image, sharp blue arcs appear. They are caused by single mirror reflections of photons from LMC X-1, which is outside the FOV.

True images of the sky were obtained by projection of each photon onto the celestial plane, taking into account the different pointing directions and roll angles. The projection takes care of the different spacing between the individual CCDs as well as for the larger size of the pixels which are furthest away from the readout nodes (Strüder et al. 2001). The result of the projection, after removing events from bright pixels and a bright column, is shown in Fig. 1. The gaps between the CCDs show up in the image, as no exposure correction was applied. The exposure map (Fig. 2) shows that these areas also received some light. The exposure map was created in a similar way as the photon image, using the vignetting curve for 1.5 keV from the XMM Users' Manual (Dahlem 1999).

Apparent in Fig. 1 is a streak-like feature from the SNR N157B. This is an artefact of the operation of the CCD, which is sensitive to X-rays also during readout. In the full frame mode, 7% of all events are recorded during this period and get a displaced position along readout direction. This effect occurs everywhere on the detector, but out-of-time event trails are evident only for bright sources. Suppressing the trails does not only improve the

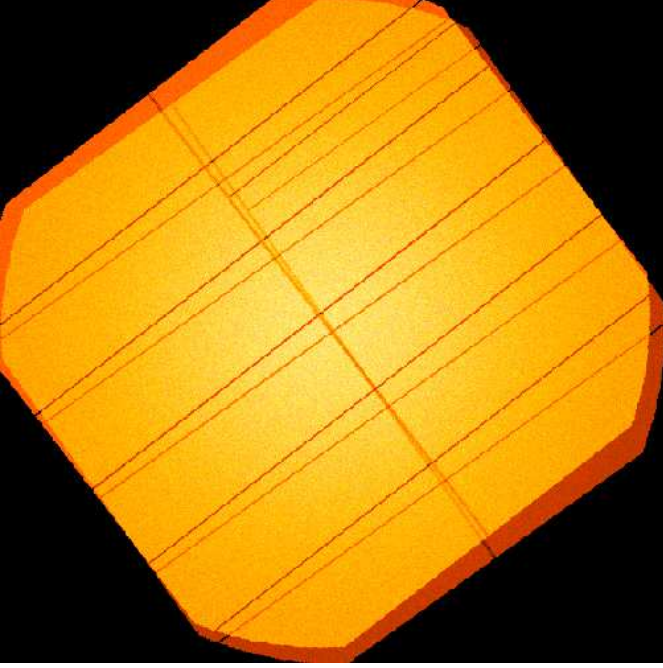


Fig. 2. Combined exposure map of all five observations. For the final image, only the inner part of the FOV was used, where the exposures overlap completely. Since the pointing position and roll angle of XMM–Newton were changed between the two sets of observations, almost all insensitive areas of the detector were exposed in the complementary observation.

image cosmetically, but also reduces local variations of the background needed to apply the source detection algorithms. In the following we describe a straightforward method to suppress the contamination by out-of-time events.

As the generation of out-of-time events is a random process, these events become uniformly distributed along each readout channel. The fraction of out-of-time events is given by the ratio of readout vs. frame time. Thus, if n is the total number of photons recorded in a particular column, the contamination n_{cont} of any pixel in this column by out-of-time events is

$$n_{\text{cont}} = \frac{t_{\text{read}}}{t_{\text{frame}} \cdot n_{\text{pix}}} \cdot n$$

where t_{read} , t_{frame} and $n_{\text{pix}} = 200$ are the readout time, the frame time and the number of pixels per column. For the full frame mode, the values are $t_{\text{read}} = 5$ ms and $t_{\text{frame}} = 73$ ms. Fig. 3 shows the contamination of Fig. 1 by out-of-time events, calculated separately for the three colour bands in detector coordinates and then projected onto the sky, so that it can be subtracted from Fig. 1.

An additional source of undesired ‘background’ in Fig. 1 are sharp, blue arcs in the lower corner, which would systematically contaminate the spectra of the diffuse soft X-ray emission in this region. These are caused by single mirror reflections of photons from the bright X-ray binary LMC X–1, which is outside the FOV. In order to

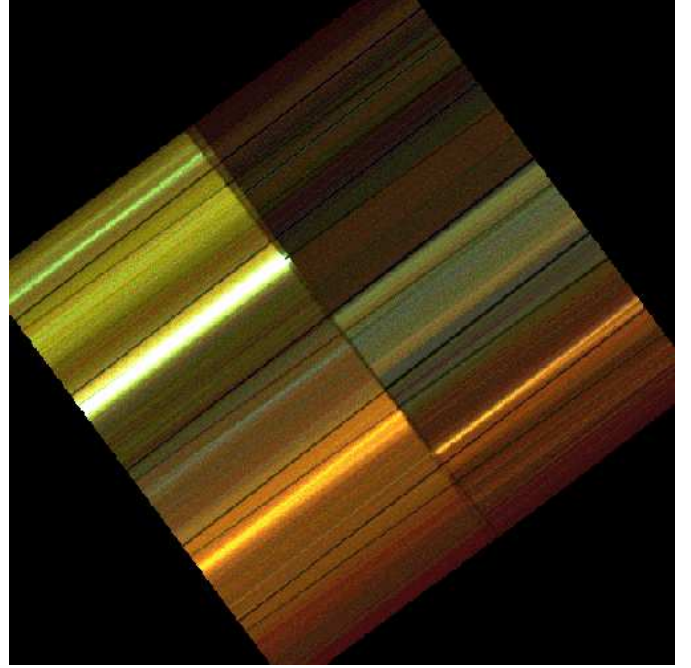


Fig. 3. Out-of-time event image of Fig. 1, constructed by distributing the events recorded in each readout column homogeneously across the column. The intensity of this image was artificially increased with respect to Fig. 1 by a factor of 20 for better visibility of these events.

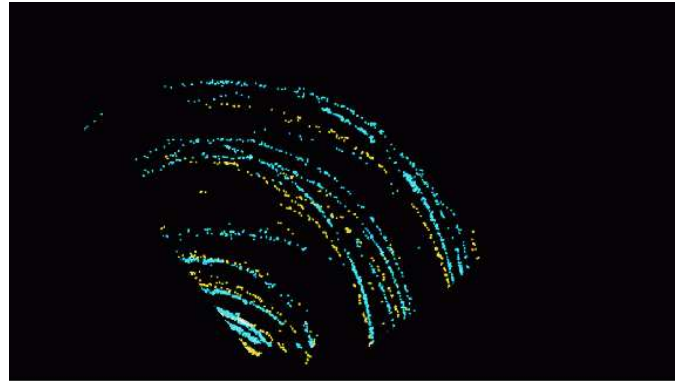


Fig. 4. Single mirror reflections of LMC X–1 in the lower corner of Fig. 1. Pixels affected during the first two observations are marked in yellow, while pixels affected during the last three observations are coded in blue. The correction was done individually for the two sets of observations.

suppress these arcs, we identified the contaminated pixels from the hard images, where they are most distinct, and flagged them (Fig. 4). For the first light image, we replaced the flux of the affected pixels by interpolated values from the adjacent pixels. This approach seems to be justified, since the extent of one pixel ($4''.13$) is considerably smaller than the half energy width of the telescope ($15''.1$), which implies that the fluxes of adjacent pixels cannot be independent of each other due to the point spread function of the telescope.

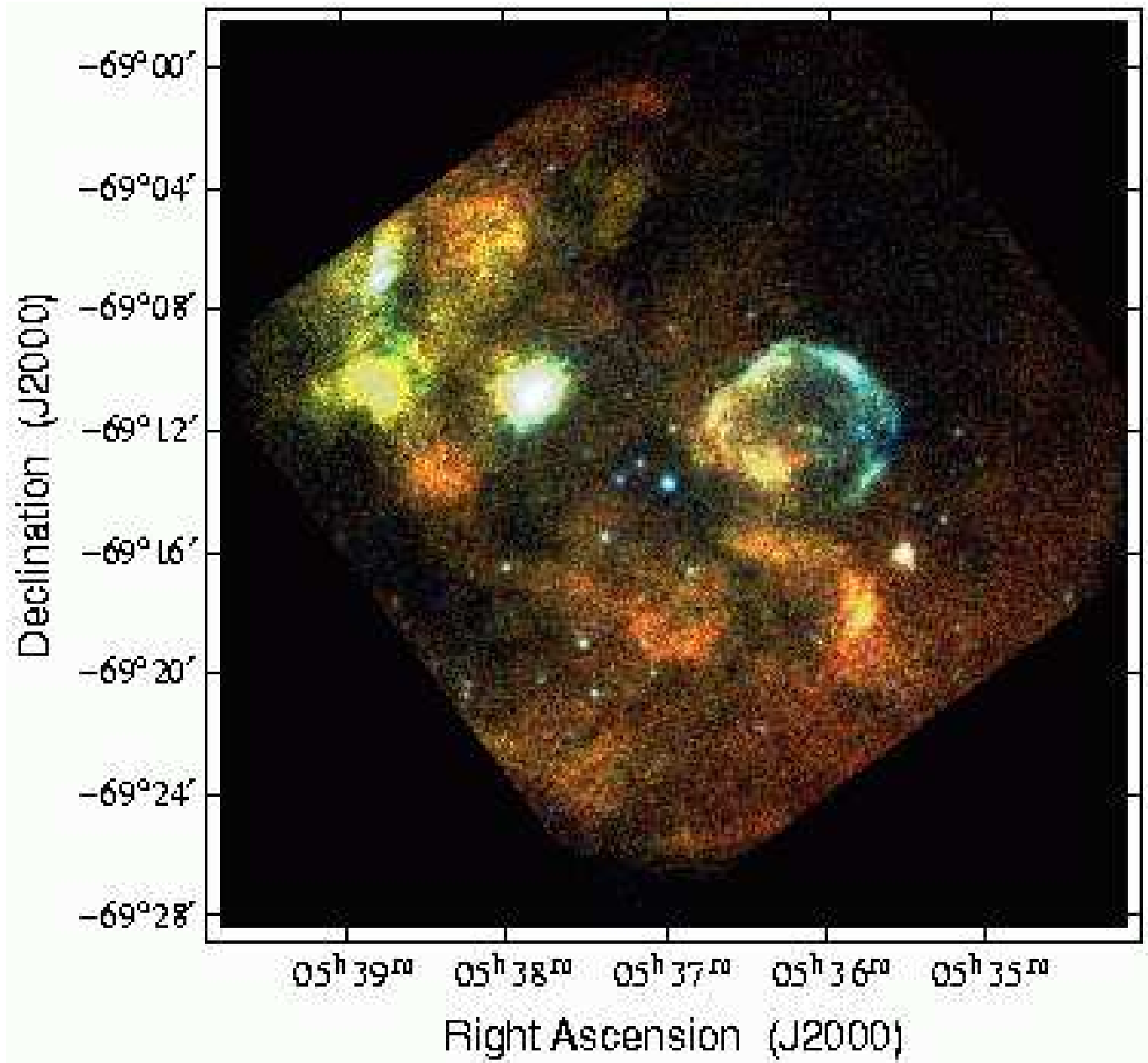


Fig. 5. Final version of the XMM–Newton EPIC pn first light X-ray colour image of the LMC, after applying all the data reductions described in the text.

A final challenge for producing the first light image was the high dynamic range in intensity, which exceeds three orders of magnitude between the diffuse extended regions of low surface brightness and the point source in N157B. Since standard techniques like logarithmic intensity coding did not yield satisfying results, we designed a special code which preserves different shades of gray for the brightest sources. The final image, boxed with an equatorial coordinate grid, is shown in Fig. 5.

3. Results and Discussion

As Fig. 5 shows, there is a wealth of different objects, point-like and extended up to 130 pc in size. The X-ray

colours show large spectral differences from object to object. Based on this image, we accumulated photons from selected regions and performed spectral investigations of various sources, to utilize the full resolving power of the EPIC pn camera. We did this separately for the three data sets which were taken with the same observational setup (filter and pointing direction), because they require different detector response matrices. The best fit was obtained by modeling each of the three count rate spectra with the same candidate source spectrum but with the individual normalization factor left as a free parameter (for details see Haberl et al. 2001). Errors were determined at $\Delta\chi^2 = +2.3$ with all parameters free.

3.1. 30 Dor C

The largest object in the field is 30 Dor C, already known from radio observations and suggested by Mills et al. (1984) to be an SNR. In X-rays it appears as a complete ring of ~ 6 arcmin diameter. The size of the shell and its colour make this remnant the first of its kind outside our Galaxy. In a separate paper (Aschenbach et al. 2001a) this unique object is investigated in detail. Close to the geometric center we detect a previously unknown point source, displayed in yellow, which emits mainly in the 0.3–1.0 keV band. If this source is in the LMC, then its luminosity is of the order of 10^{33} erg s $^{-1}$, and it might be the compact remnant of 30 Dor C, either a neutron star or a black hole.

3.2. SN 1987A

Approximately 2 arcmin to the south-west of the shell border is the well-known SN 1987A. The XMM-Newton observations are very important with respect to both, the light curve and the X-ray spectrum, refining current models of SN 1987A. Both aspects are presented and discussed in an accompanying paper by Aschenbach et al. (2001b).

3.3. Active Galactic Nuclei behind the LMC

A number of point sources have been discovered, displayed as blue dots in Fig. 5, the brightest of which is seen close to the image center. These sources have power law spectra and show strong low energy absorption. Both, the spectra and the fact that the central source is associated with a radio point source, indicate that we see background sources, probably AGN, Nuclei, through and far beyond the LMC. A detailed analysis of these new X-ray sources is presented in an accompanying paper by Haberl et al. (2001).

3.4. N157B

By far the brightest object in the field is the SNR N157B, located halfway from the image center to the edge in north-easterly direction. After the discovery of the 16 ms pulsar (Marshall et al. 1998, Wang & Gotthelf 1998b) N157B has been classified as a Crab-like remnant with a central pulsar and a surrounding synchrotron nebula. In a preceding paper Wang & Gotthelf (1998a) showed that the spectrum is dominated by a power law with an indication of some thermal emission. The XMM-Newton spectrum of N157B (Fig. 6) demonstrates convincingly for the first time the presence of emission lines at low energies, proving the presence of a thermal component. A model comprising two thermal components and a power law gives an acceptable fit to the data. Formally, ionization equilibrium models like Raymond-Smith (RS; Raymond & Smith 1977) or non equilibrium ionization models (NEI; Hamilton et al. 1983) of XSPEC used for the thermal components at low energies cannot be discriminated.

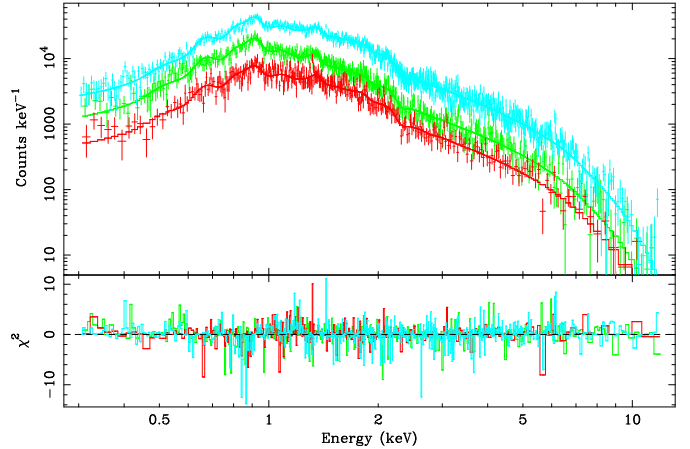


Fig. 6. EPIC pn X-ray spectra of N157B for the three data sets with the same observational setup. The histograms represent the best fit model simultaneously applied to the spectra.

Fig. 6 shows the best fit two temperature RS models with a power law model added. The temperatures are $0.37^{+0.11}_{-0.05}$ keV and 0.12 ± 0.01 keV, and the photon index of the power law is 2.83 ± 0.03 . With an assumed hydrogen equivalent photoelectric absorption of $6 \cdot 10^{20}$ H-atoms cm $^{-2}$ for the galactic foreground, we derive an additional H-equivalent column density of $(1.94 \pm 0.04) \cdot 10^{22}$ H-atoms cm $^{-2}$ for the absorption in the LMC, taking elemental abundances of 0.5 solar into account. To fit the Mg emission line at 1.3 keV clearly seen in the spectra, an overabundance of 1.3 solar is required (for the cooler component). The NEI model yields similar values for the absorption, the Mg abundance and the power law slope, but different temperatures (0.24 and 0.10 keV).

The existence of the additional two-temperature thermal component suggests that N157B is not a Crab-like remnant but a composite remnant with an X-ray bright pulsar and synchrotron nebula but relatively faint thermal shell. The analysis of the thermal component, to be done in a separate paper, will be used to check for instance the consistency of the age derived from a Sedov-type approach with the pulsar characteristic spin-down age of $P/(2\dot{P}) \sim 5000$ ys (Wang & Gotthelf 1998b).

The power law component in the spectrum of N157B which has been discovered by Wang & Gotthelf (1998a) using ROSAT PSPC and ASCA SIS data gives a photon index of 2.3 ± 0.1 . The EPIC pn best fit value for the index is 2.83 ± 0.03 . N157B has been compared with the Crab. Both the Crab pulsar and the N157B 16 ms pulsar (Marshall et al. 1998) show a flat power law spectrum with a photon index of 1.5 and 1.6 ± 0.3 , respectively. The spectrum of the Crab nebula is steeper by 0.5, generally believed to be due to synchrotron losses. If the spectrum of N157B would have a similar difference of ~ 0.5 between the pulsar and the nebula spectrum as suggested by the analysis of Wang & Gotthelf, the analogy with the Crab would be convincing. If on the other hand the EPIC pn power law slope is a better representation of the spectrum,

the analogy with the Crab is clearly violated and other acceleration and loss processes have to be considered. We note that the analysis of power law dominated spectra like in AGN show just minor discrepancies in the spectral index between ASCA and EPIC pn. Because of the steep spectrum of the nebula the physical conditions, either the electron injection spectrum, the electron transport speed or the magnetic field distribution, are likely to be different from those prevailing in the Crab.

3.5. The Honeycomb nebula

In Fig. 5, X-ray emission from the Honeycomb nebula is seen 1 arcmin south-east of SN 1987A. The emission of the bright orange patch can be modeled by a thermal plasma with a temperature of 0.19 ± 0.02 keV, superimposed on a power law of index 3.6 ± 0.6 . Increased Ne and Mg abundances (~ 2 times solar) are indicated. The hydrogen equivalent LMC absorption to this SNR is $(2.2 \pm 0.9) \cdot 10^{21}$ H-atoms cm^{-2} . Fig. 7 shows the three EPIC pn spectra together with the best fit model.

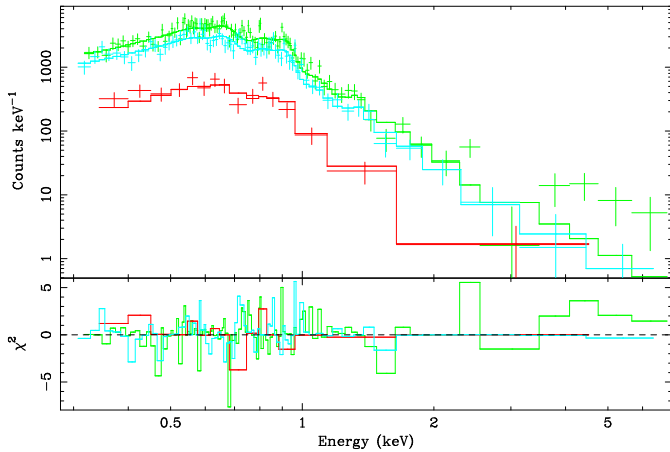


Fig. 7. Same as Fig. 6 for the Honeycomb nebula.

3.6. Interstellar medium in the LMC

The north-western part of Fig. 5 appears remarkably dark and empty. But when we extract a spectrum from a 44 arcmin^2 region north of 30 Dor C where no point sources and no out-of-time events from 30 Dor C affect the data, we clearly see thermal emission. The temperature appears to differ from place to place over a range from ~ 0.1 keV and ~ 0.3 keV, as was already concluded from ROSAT PSPC spectra (Sasaki et al. 2001). But for the first time we detect emission lines of oxygen, neon, magnesium and silicon (Fig. 8). To fit the spectrum, we subtracted the background in a preliminary way, using source free areas from other EPIC pn observations. The resulting spectrum is well represented by a $0.3^{+0.05}_{-0.2}$ keV RS type model with overabundances in O, Ne, Mg and Si of 1.6 ± 0.7 , 5.4 ± 1.5 , 6.6 ± 2.5 and 8.9 ± 7.4 solar, respectively,

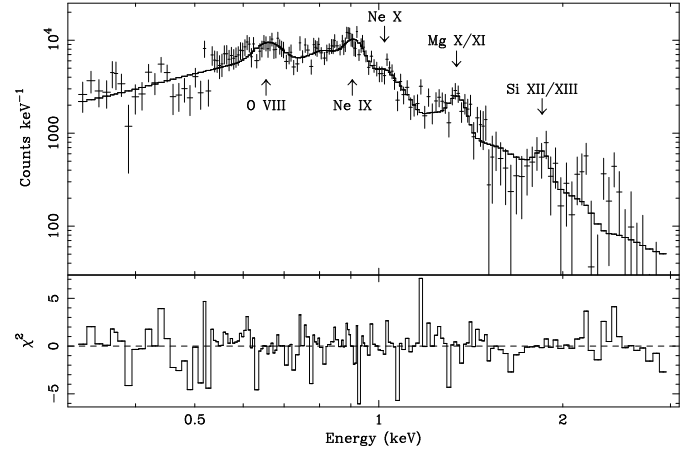


Fig. 8. EPIC pn X-ray spectrum of the faint, diffuse emission in the north of Fig. 5, accumulated from the last two observations with thin filter.

which is surprising in view of the generally low metallicity of the LMC.

Acknowledgements. The XMM-Newton project is supported by the Bundesministerium für Bildung und Forschung/Deutsches Zentrum für Luft- und Raumfahrt (BMFT/DLR), the Max-Planck Society and the Heidenhain-Stiftung.

References

- Aschenbach, B. et al. 2001a, submitted to Nature
 Aschenbach, B. et al. 2001b, submitted to A&A
 Briel, U. G., Aschenbach, B., Balasini, M. et al. 2000, SPIE 4012, 154
 Dahlem, M., 1999, XMM-PS-GM-17, 20
 Dennerl, K., Briel, U. G., Haberl, F. et al. 1999, SPIE 3765, 232
 Haberl, F., Dennerl, K., Filipović, M. D. et al. 2001, A&A, 365 (this issue)
 Hamilton, A. J. S., Sarazin, C. L., Chevalier, R. A., 1983, ApJS 51, 115
 Jansen, F., Lumb, D., Altieri, B. et al. 2001, A&A, 365 (this issue)
 Long, K. S., Helfand, D. J., Grabelsky, D. A., 1981, ApJ 248, 925
 Marshall, F. E., Gotthelf, E. V., Zhang, W., Middleditch, J., Wang, Q. D., 1998, ApJ 499, L179
 Mills, B. Y., Turtle, A. J., Little, A. G., Durdin, J. M., 1984, Aust. J. Phys. 37, 321
 Raymond, J. C., Smith, B. W., 1977, ApJS 35, 419
 Sasaki, M., Haberl, F., Pietsch, W., 2001, in: X-ray Astronomy 2000, Palermo, in press
 Strüder, L., Briel, U. G., Dennerl, K. et al. 2001, A&A, 365 (this issue)
 Trümper, J., Hasinger, G., Aschenbach, B. et al. 1991, Nat 349, 579
 Turner, M. J. L., Abbey, A., Arnaud, M. et al. 2001, A&A, 365 (this issue)
 Wang, Q. D. & Gotthelf, E. V., 1998a, ApJ 494, 623
 Wang, Q. D. & Gotthelf, E. V., 1998b, ApJ 509, L109
 Watson, M. G., Auguères, J.-L., Ballet, J. et al. 2001, A&A, 365 (this issue)